Received: 12 September 2023 | Revised: 16 October 2023 | Accepted: 27 October 2023

DOI: 10.1002/pro.4826

RESEARCH ARTICLE

Nucleocapsid proteins from human coronaviruses possess phase separation capabilities and promote FUS pathological aggregation

Hui Dong[1] | **Hong Zhang**[1] | **Julie Jalin**[1] | **Ziqi He**[2] | **Runhan Wang**[1] | **Leqi Huang**[1] | **Zibo Liu**[1] | **Shenqing Zhang**[3,4] | **Bin Dai**[1] | **Dan Li**[3,4]

[1]School of Life Sciences and Biotechnology, Shanghai Jiao Tong University, Shanghai, China

[2]College of Stomatology, Shanghai Jiao Tong University, Shanghai, China

[3]Bio-X Institutes, Key Laboratory for the Genetics of Developmental and Neuropsychiatric Disorders, Ministry of Education, Shanghai Jiao Tong University, Shanghai, China

[4]Zhangjiang Institute for Advanced Study, Shanghai Jiao Tong University, Shanghai, China

Correspondence
Bin Dai, School of Life Sciences and Biotechnology, Shanghai Jiao Tong University, Shanghai, 200240, China.
Email: lidan2017@sjtu.edu.cn

Dan Li, Bio-X Institutes, Key Laboratory for the Genetics of Developmental and Neuropsychiatric Disorders, Ministry of Education, Shanghai Jiao Tong University, Shanghai 200030, China.
Email: daibin@sjtu.edu.cn

Present address
Hui Dong, Interdisciplinary Research Center on Biology and Chemistry, Shanghai Institute of Organic Chemistry, Chinese Academy of Sciences, Shanghai, China.

Funding information
National Natural Science Foundation of China, Grant/Award Number: 32170683

Abstract

The nucleocapsid (N) protein is an essential structural component necessary for genomic packaging and replication in various human coronaviruses (HCoVs), such as SARS-CoV-2 and MERS-CoV. Recent studies have revealed that the SARS-CoV-2 N protein exhibits a high capacity for liquid–liquid phase separation (LLPS), which plays multiple roles in viral infection and replication. In this study, we systematically investigate the LLPS capabilities of seven homologous N proteins from different HCoVs using a high-throughput protein phase separation assay. We found that LLPS is a shared intrinsic property among these N proteins. However, the phase separation profiles of the various N protein homologs differ, and they undergo phase separation under distinct *in vitro* conditions. Moreover, we demonstrate that N protein homologs can co-phase separate with FUS, a SG-containing protein, and accelerate its liquid-to-solid phase transition and amyloid aggregation, which is closely related to amyotrophic lateral sclerosis. Further study shows that N protein homologs can directly bind to the low complexity domain of FUS. Together, our work demonstrates that N proteins of different HCoVs possess phase separation capabilities, which may contribute to promoting pathological aggregation of

Abbreviations: AD, Alzheimer's disease; ALS, amyotrophic lateral sclerosis; CTD, C-terminal dimerization domain; E, envelope; FRAP, fluorescence recovery after photobleaching; FTD, frontotemporal dementia; HCoVs, human coronaviruses; HiPPS, high-throughput protein phase separation; IDRs, intrinsically disordered regions; LC, low complexity; LKR, linker region; LLPS, liquid–liquid phase separation; M, membrane; MERS-CoV, Middle East respiratory syndrome coronavirus; N protein, nucleocapsid protein; Nsp, non-structural proteins; NTD, N-terminal domain; PD, Parkinson's disease; RBP, RNA-binding protein; RTCs, replication transcription complexes; S, spike; SARS-CoV-2, severe acute respiratory syndrome coronavirus-2; SG, stress granule; TEM, transmission electron microscopy.

Hui Dong and Hong Zhang contributed equally to this work.

Reviewing Editor: John Kuriyan

host proteins and disrupting SG homeostasis during the infection and replication of various HCoVs.

KEYWORDS

FUS protein, human coronaviruses, nucleocapsid proteins, phase separation

1 | INTRODUCTION

The COVID-19 pandemic, a global health crisis, is caused by the highly contagious severe acute respiratory syndrome coronavirus 2 (SARS-CoV-2), which belongs to the subfamily Coronavirinae and is one of the seven pathogenic Human Coronaviruses (HCoVs) identified so far (Wu et al., 2020; Yang and Rao, 2021; Coronaviridae Study Group of the International Committee on Taxonomy of Viruses, 2020; Chen et al., 2020). The other six HCoVs include SARS-CoV, Middle East respiratory syndrome coronavirus (MERS-CoV), HCoV-HKU1, HCoV-OC43, HCoV-229E, and HCoV-NL63. SARS-CoV, SARS-CoV-2, and MERS-CoV have caused public health emergencies in the last two decades (Drosten et al., 2003; Zaki et al., 2012; Fung and Liu, 2019), while HCoV-HKU1/OC43/229E/NL63 cause mild respiratory tract illnesses (Fung and Liu, 2019). All HCoVs are enveloped, positive-sense, single-stranded ~30 kb RNA viruses. These genomes encode sixteen nonstructural proteins (nsp1–nsp16) required for viral replication and pathogenesis (Zhou et al., 2020; V'Kovski et al., 2021; Snijder et al., 2006), four structural proteins including spike (S), envelope (E), membrane (M), and nucleocapsid (N), and seven to eight auxiliary proteins (V'Kovski et al., 2021; Chang et al., 2014). The N protein is an essential structural protein that acts as a crucial player in viral genomic packaging and replication (Snijder et al., 2006; Chen et al., 2007). It is a multidomain RNA-binding protein (RBP) with a molecular weight ranging from 42 to 48 kDa in different HCoVs (Chang et al., 2014; Chan et al., 2020). N protein homologs derived from different HCoVs share similar functional modular organization, making them conserved throughout HCoV's evolution (Zhou et al., 2020; Chang et al., 2014).

Recent studies have shown that the N protein of SARS-CoV-2 exhibits a high ability for liquid–liquid phase separation (LLPS), which may play multiple roles in viral infection and replication (Zheng et al., 2021; Lu et al., 2021; Cubuk et al., 2021; Luo et al., 2021; Savastano et al., 2020; Iserman et al., 2020; Dolliver et al., 2022; Cascarina and Ross, 2020). These roles include (1) condensing the viral genome, (2) regulating ribonucleoprotein assembly in the viral lifecycle, and (3) disrupting the dynamic assembly of stress granules (SGs) by interfering with SG-containing proteins such as TDP-43, FUS, and hnRNPA1 (Luo et al., 2021; Li et al., 2022). Importantly, the N protein can co-phase separate with FUS and promote its pathological amyloid aggregation, which is closely associated with neurodegenerative diseases (NDs) such as amyotrophic lateral sclerosis (ALS) and frontotemporal dementia (FTD) (Li et al., 2022). This implies a possible link between SARS-CoV-2 infection, brain invasion, and NDs. Since the N protein LLPS plays an essential role in the infection caused by SARS-CoV-2, it would be valuable to investigate whether this property is inherent and commonly shared by the N proteins from all seven different HCoVs.

In this study, we systematically explored the LLPS capability of all seven homologous N proteins of different HCoVs by using a high-throughput protein phase separation (HiPPS) assay. Our results demonstrate that all N proteins can undergo LLPS *in vitro*, but each exhibits a distinct LLPS profile. We further found that the different N proteins can directly bind to the low complexity domain of FUS, co-phase separate with it, and promote its amyloid fibrillation to varying degrees. Our findings suggest that N proteins of HCoVs share a similar mechanism for promoting pathological protein aggregation, and their LLPS plays a vital role in this process.

2 | RESULTS

2.1 | Phase separation is an intrinsic property shared by different N proteins

Recognizing the importance of protein phase separation in various processes, we systematically examined and compared the phase separation capability of homologous N proteins from seven different HCoVs. Each N protein contains three conserved domains, including a folded N-terminal domain (NTD) involved in RNA packaging, a folded C-terminal dimerization domain (CTD), and an intrinsically disordered central linker region (LKR) (Chang et al., 2014). Sequence alignment showed that SARS-CoV-2 N protein shares ~90% identity and 93% similarity with SARS-CoV N protein, and hold ~35%–50% identity and ~45%–60% similarity to the remaining five homologous N proteins (Figures 1a and S1).

Importantly, the intrinsically disordered regions (IDRs) of all seven homologous N proteins exhibited high propensity for LLPS, as predicted by PONDR VSL2 predictor (Obradovic et al., 2003) (Figures 1b and S1).

We purified the seven recombinant HCoV N proteins, and investigated their LLPS profiles by using a well-established HiPPS assay *in vitro* (Li et al., 2022). Microscopic images of each well were recorded and scored for calculating the protein phase separation (PPS) score of each individual protein. Remarkably, all seven HCoV N proteins underwent phase separation in the 96-well plate with different LLPS scores (Figure 1c), demonstrating

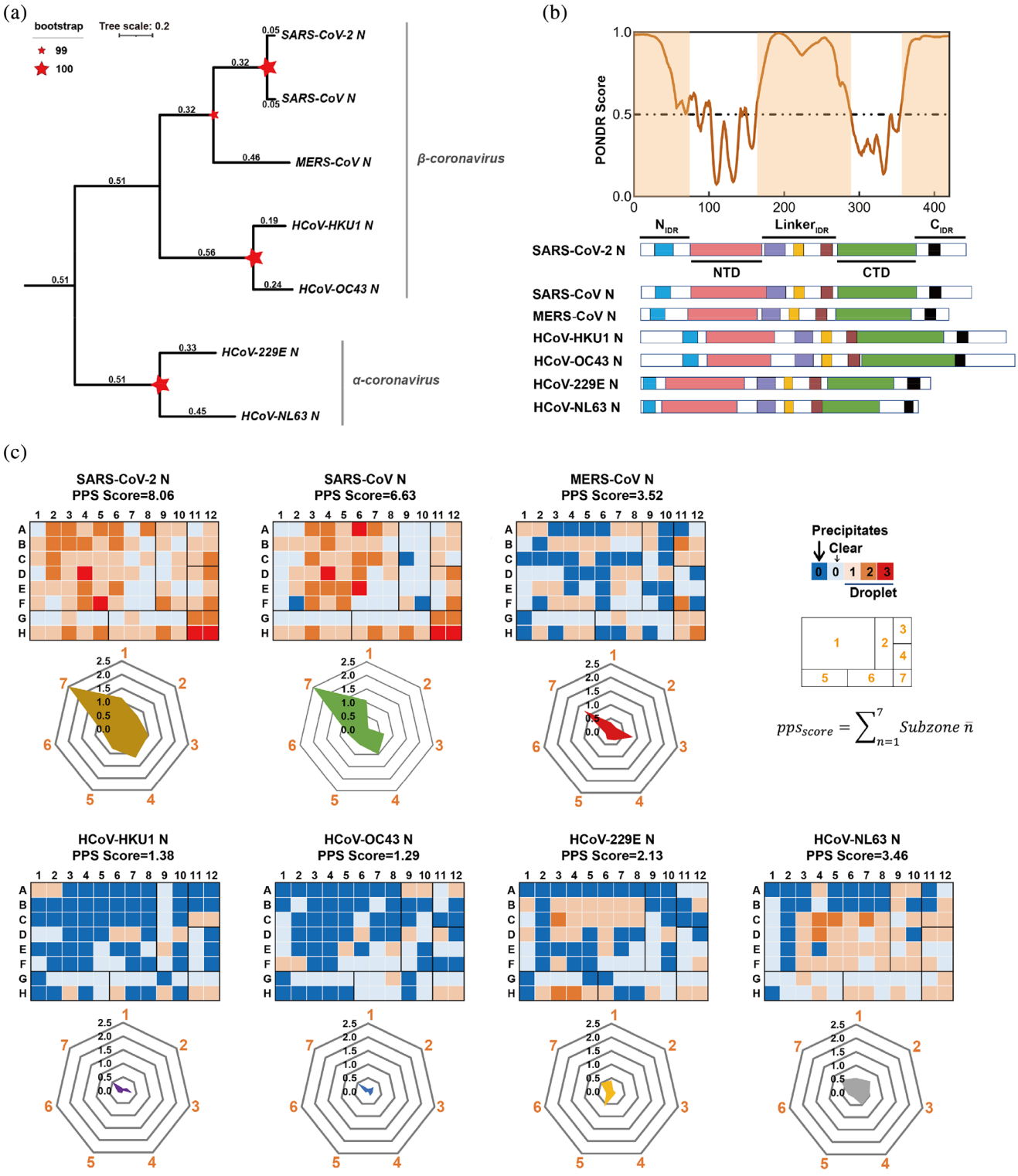

$$pps_{score} = \sum_{n=1}^{7} Subzone\ \bar{n}$$

FIGURE 1 Legend on next page.

that phase separation is a common property shared by different N proteins.

Furthermore, we compared the radar graph of different N proteins, calculated from seven sub-zones containing different groups of LLPS conditions (e.g., pH, salt, positive-charged agent, and crowding agent) from the 96 conditions (Table S1). Notably, different N proteins exhibited distinct phase separation profiles. SARS-CoV-2-N, previously identified to phase separate (Lu et al., 2021; Cubuk et al., 2021), had the strongest LLPS ability with a PPS score of 8.06 and was able to undergo phase separation under almost all tested conditions (Figure 1c). SARS-CoV N had the second-highest PPS score of 6.63 (Figure 1c). In contrast, HCoV-HKU1 N and HCoV-OC43 N had a relatively weak LLPS ability, with a PPS score of 1.38 and 1.29, respectively, and could only undergo phase separation in less than 15% of the conditions (Figure 1c). Interestingly, all seven N proteins could be induced to undergo phase separation in the presence of the crowding agent PEG3,350 within sub-zone 7 (Figure 1c). SARS-CoV-2 N and SARS-CoV N possess a relatively broad phase separation space and are able to phase separate at a wide pH range (3.5–8.5) and under various salts concentrations. The other N proteins, however, respond markedly differently to various conditions: they undergo phase separation under PEG3350 but aggregate and precipitate when exposed to certain salt conditions (zinc, magnesium) due to strong interactions. This result revealed that while all seven N proteins are capable of phase separation, their propensities varied significantly (Figure 1C), highlighting that not all N proteins are alike in their phase separation capacities. Moreover, SARS-CoV-2 N, SARS-CoV N, MERS-CoV N, and HCoV-NL63 N could undergo phase separation with the addition of homopolymeric RNA (PolyU, PolyR) in subzone 3 and 4 (Figure 1c). Previous studies showed that single-stranded RNA can promote LLPS of SARS-CoV-2 N, which may be involved in viral genome packaging (Cubuk et al., 2021; Zeng et al., 2020; Chang et al., 2009). Thus, RNA-facilitated N protein phase separation may be commonly used for viral genomic RNA packing in different HCoVs.

2.2 | N proteins form dynamic liquid-like droplets *in vitro*

To further examine the dynamic features of droplets formed by different N proteins, we labeled N protein with the fluorescence dye QSY7. Fluorescent and differential interference contrast (DIC) imaging data showed that the N protein formed spherical droplets in the presence of PEG3350 (Figure 2a). Turbidity measurement further showed an increase in the OD_{600} value to varying degrees for all seven different N proteins (Figure 2b). Among them, HCoV-NL63 N, HCoV-HKU1 N, and HCoV-229E N showed relatively low OD_{600} values, indicating a decreased tendency for phase separation under comparable conditions (Figure 2b). Moreover, the fluorescence recovery after photobleaching (FRAP) assay showed that the fluorescence signal within the droplets formed by different N proteins rapidly recovered to 70%–75% within 1 min after bleaching (Figure 2c). Thus, different N proteins can undergo LLPS to form liquid-like droplets with high interior dynamics.

2.3 | N protein co-phase separates with FUS and promotes droplet maturation

Previous studies showed that SARS-CoV-2 N can co-phase separate with several SG-containing proteins, including FUS and TDP-43, and promote their aggregation, which is believed to be associated with the solidification and dysfunction of host SGs during virus infection (Li et al., 2022; Perdikari et al., 2020). We next asked

FIGURE 1 LLPS is a general property shared by N proteins from seven different human coronavirus. (a) The phylogenetic tree was generated from primary sequence of the seven homologous N proteins by using ClusterW (http://align.genome.jp) and plotted using a Neighbor-Joining algorithm. Tree scale and bootstrap value are indicated. (b) IDR score (SARS-CoV-2 N as a represent) and the domain organization of the N proteins from human coronaviruses. PONDR VSL2 predictor23 was used for calculating the IDR score. The region consisting of residues with score value higher than 0.5 is considered to be IDR (highlighted area in orange). N protein contains three putatively disordered regions: a globular N-terminal tail, a C-terminal tail and a central linker region. The homologous regions in the IDR are highlight in different color-zone: AXXITFADSD motif (blue), FYAEGSXG motif (purple), SR-rich motif(orange), LALLXL---QQ motif (brown), K--Q--VTL motif (black). (c) Characterization of different N proteins from HCoVs for their LLPS abilities by HiPPS profiling. HiPPS profiles (top) and radar graph (bottom) of each N protein are shown. 50 μM of each N protein was examined at room temperature. The parameter and equation for calculating PPS scores are shown on the upper right. Values in the radar graph represent the average grades of each square sub-zones in the HiPPS profiles; The profiling condition in sub-zones 1–7 shown on the upper right, includes: different crowding agents (sub-zone 1); high concentration salts (sub-zone 2); PolyR (sub-zone 3); PolyU/heparin (sub-zone 4); divalent salts (sub-zone 5); monovalent salts (sub-zone 6); PEG 3350 gradient (sub-zone 7). PPS score, protein phase separation score.

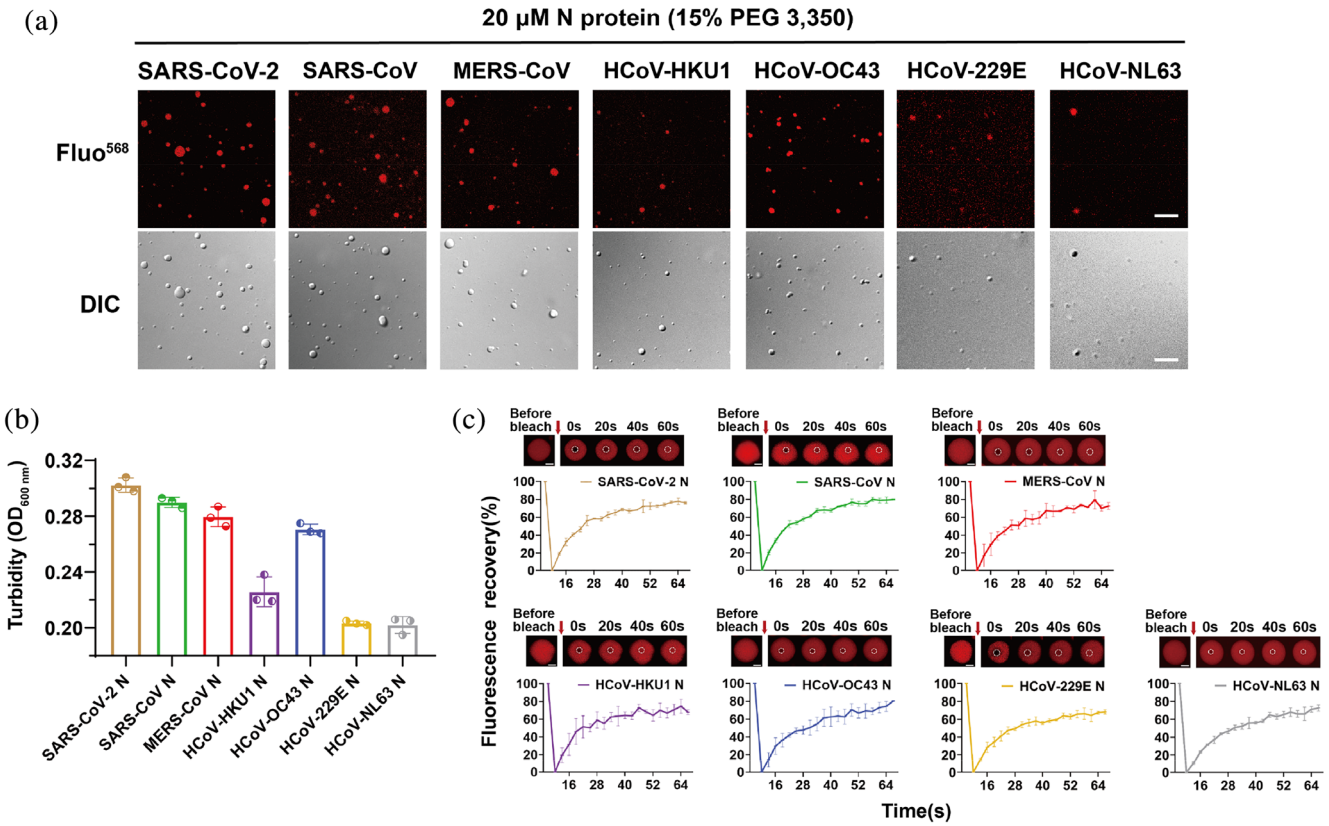

FIGURE 2 N protein undergoes LLPS *in vitro* and exhibits dynamic features in droplets. (a) Microscopic images of N protein droplets in the presence of PEG3350 in the buffer containing 50 mM Tris–HCl, pH 7.5 and 150 mM NaCl. DIC, differential interference contrast microscopy. QSY7 is a chemical fluorescence dye to label N protein. Scale bar, 10 μm. (b) Turbidity measurement of the N protein samples shown in panel (a). Turbidity measurements were conducted at 600 nm. Data are shown as mean ± SD with $n = 3$. (C) FRAP of QSY7-labeled N proteins. FRAP curves and montages of each N protein droplet are shown. Dashed circles indicate the photo-bleached spot. The arrow indicates the action of bleaching. The graph (bottom) shows the recovery fraction as the function of time. Data are shown as mean ± SD with $n = 3$ individual droplets. Scale bar, 2 μm.

whether different N proteins are able to co-phase separate with the SG-containing protein FUS and influence its amyloid aggregation. Notably, fluorescent microscopic imaging showed that, similar to SARS-CoV-2 N, the other six N proteins can spontaneously condense into FUS droplets for co-phase separation (Figure 3a). To further explore whether co-phase separation can promote FUS droplet maturation, we prepared FUS with enhanced green fluorescent protein (EGFP) fused at the C-terminus (FUS-EGFP). Consistent with previous observations (Gu et al., 2020; Li et al., 2022), FUS-EGFP can spontaneously form liquid-like droplets that remain dynamic for up to 6 h (Figure 3b). Remarkably, the addition of different N proteins dramatically altered the morphology of the FUS droplet and induced the formation of fibrillar structures growing out of the droplets after co-incubation for 6 h. The addition of SARS-CoV N, HCoV-HKU1 N, and HCoV-229E N led to the formation of less spherical droplets with increasing numbers of fibril-like structures growing out of the droplets. This suggests that these three N protein homologs display stronger activity in stimulating the maturation of FUS droplets. Moreover, the FRAP results showed that the spiky FUS droplets induced by N proteins exhibit largely impaired internal mobility, and the fluorescence signal of FUS-EGFP can hardly recover after bleaching (Figures 4c and S4). Together, our results demonstrate that different N proteins can not only co-phase separate with FUS but also promote the liquid-to-solid maturation process of FUS with varying activities.

2.4 | N proteins directly bind to FUS-LC and promote its amyloid aggregation

As FUS amyloid aggregation is the key event driving FUS liquid-to-solid phase transition (Patel et al., 2015; Rhoads et al., 2018; Naumann et al., 2018; Mathieu et al., 2020), we directly assessed the influence of different N proteins on FUS aggregation by performing a thioflavin T (ThT) fluorescence assay and negative-staining transmission electron microscopy (TEM). We purified the N-terminal

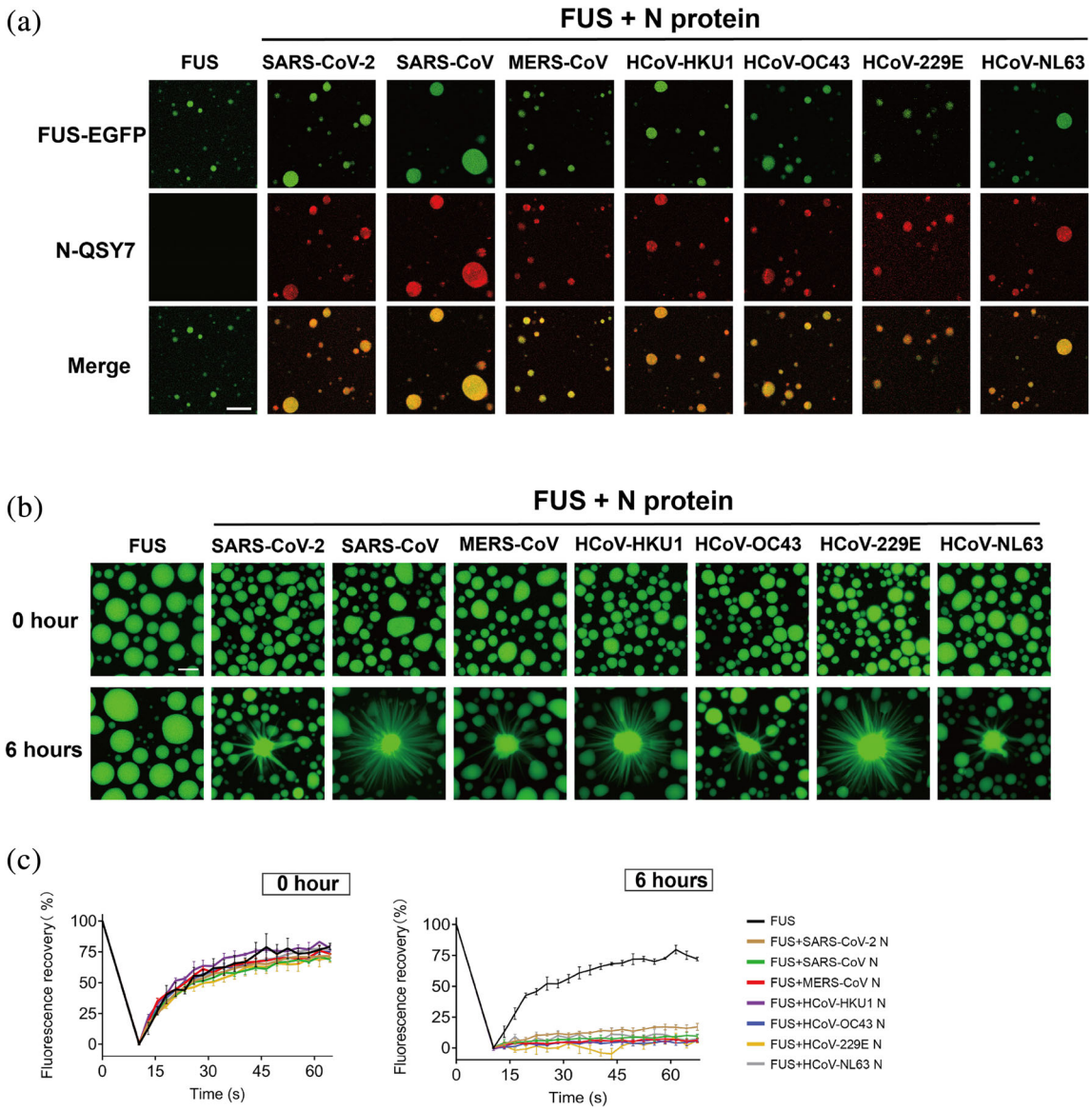

FIGURE 3 Different N proteins co-phase separate with FUS and solidify its liquid-like droplets. (a) Fluorescence images of co-phase separation of N protein with FUS. The concentration of FUS is 10 μM, and the molar ratio of FUS to N protein is 10:1. LLPS buffer:50 mM Tris–HCl, pH 7.5, 150 mM NaCl. EGFP is a fluorescence tag. QSY7 is fluorescence dye. Scale bar, 10 μm. (b) Representative images of the liquid-like droplets of FUS-EGFP in the absence or presence of different N proteins in a maturation process within 6 h. Scale bar, 10 μm. (c) FRAP curves of FUS-EGFP droplet samples validated in (b) taken at the incubation time of 0 h (left) and 6 h (right). Data are shown as mean ± SD with $n = 3$ independent replicates.

LC domain of FUS (FUS-LC), which is reported to be responsible for mediating FUS aggregation (Kato et al., 2012; Sun et al., 2022; Murray et al., 2017). It was then incubated with or without different N proteins for aggregation. Strikingly, all seven N proteins effectively enhanced the ThT fluorescence intensities and shortened the lag time of the ThT kinetic curves of FUS aggregation in a dose-dependent manner (Figures 4 and S5). However, different N proteins exhibited distinct activities in promoting FUS-LC aggregation. Specifically, N proteins of HCoV-OC43 and HCoV-HKU1 showed the strongest activity in promoting FUS-LC aggregation, shortening the lag time of FUS-LC fibril nucleation by over 30 h. In contrast, SARS-CoV-2 N only shortened the lag time of FUS-LC fibril nucleation by approximately 12 h. TEM imaging confirmed the formation of typical FUS fibrils in these ThT-positive samples (Figure 4a). As a control, N proteins did not form amyloid fibrils on their own under the same conditions (Figure S6).

Lastly, we sought to measure the direct interaction between FUS-LC and the seven N proteins using Bio-Layer interferometry (BLI) assay. FUS-LC was

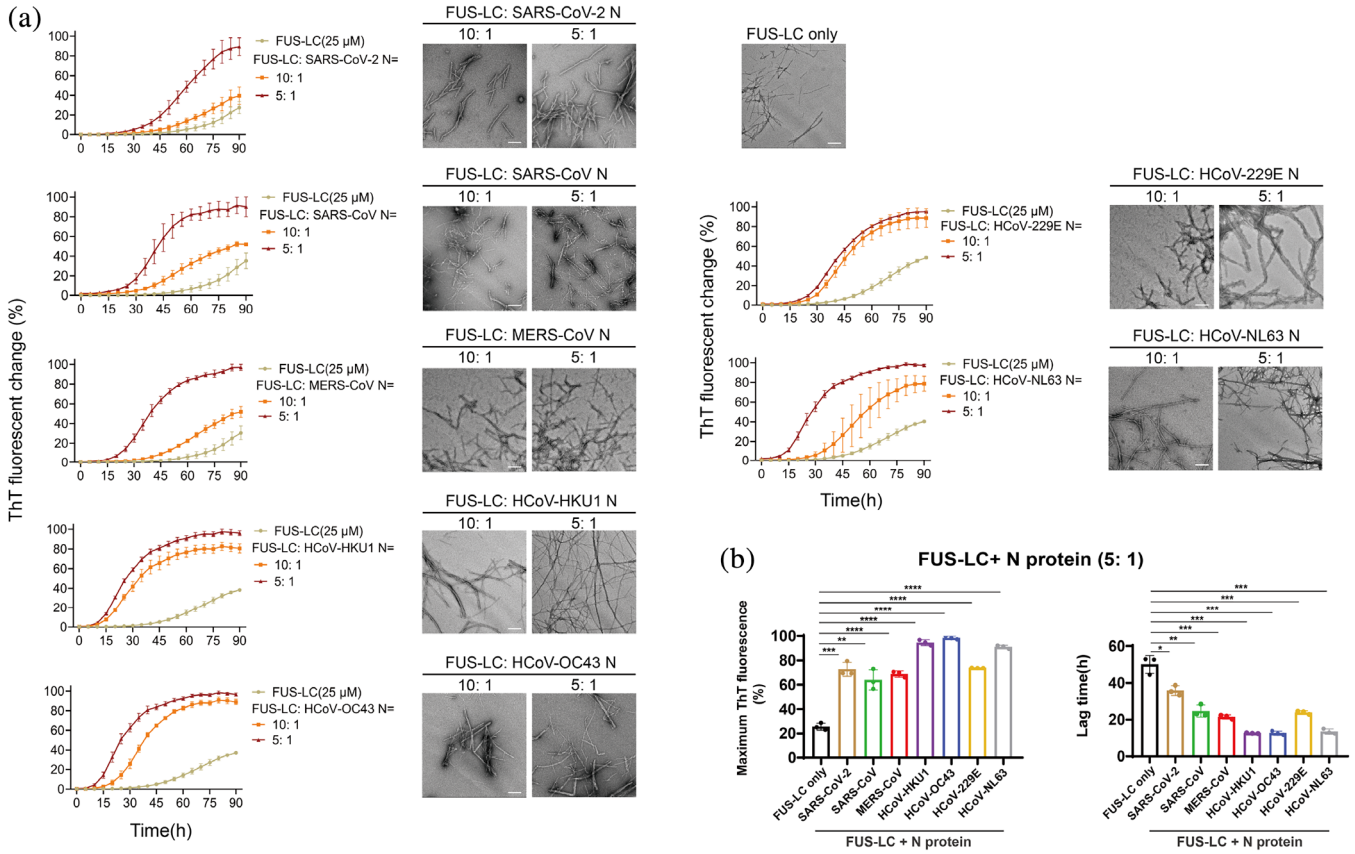

FIGURE 4 N protein promotes amyloid aggregation of FUS-LC. (a) ThT kinetic assay and NS-TEM image of amyloid fibril formation of FUS-LC. Protein concentration of FUS-LC and the molar ratio of FUS: N protein is indicated. Buffer for FUS-LC amyloid formation: 50 mM Tris–HCl, pH 7.5 and 150 mM NaCl, 50 μM ThT and 0.05% NaN_3. Data are shown as mean ± SD with $n = 3$ independent replicates. TEM images of samples were taken at the time point of 90 h incubation. Scale bar, 200 nm. (b) Comparison of seven N proteins on their ability to promote FUS amyloid aggregation. Maximum ThT fluorescence intensity after 90 h incubation (left) and the lag time (right) of fibrillation of 25 μM FUS-LC in the presence of 5 μM N protein is shown. Data are shown as mean ± SD with $n = 3$ independent replicates. Student's *t* test, $^*p < 0.05$; $^{**}p < 0.01$; $^{***}p < 0.001$; $^{****}p < 0.0001$.

immobilized on biosensor tips, and the association and dissociation curves were measured in the presence and absence of five different concentrations of N protein to calculate the equilibrium dissociation constant (K_D) between FUS-LC and the N protein. The BLI results showed that different N proteins can bind to FUS-LC with K_D values ranging from 30 to 100 nM, which is within the same order of magnitude. Among them, FUS-LC/SARS-CoV-2 N exhibited the strongest binding with a K_D value of 34 nM, and HCoV-NL63 N had the highest K_D value of 100 nM (Figure 5). Together, these data demonstrate that different N proteins can directly bind to FUS-LC and promote its amyloid aggregation.

3 | DISCUSSION

Recently, numerous proteins have been identified that demonstrate the ability to undergo phase separation, which plays a role in forming various biomolecular condensates involved in diverse biological processes (Banani et al., 2017; Decker and Parker, 2012; Jung et al., 2020; Quiroz et al., 2020; Su et al., 2016; Zeng et al., 2018; Zhang et al., 2018, 2020, 2020; Zhu et al., 2022). Increasing evidence indicates that LLPS of the N protein from SARS-CoV-2 is involved in forming condensed protein-nucleic acid compartments and packaging its genome into new virions, a crucial step in the virus' life cycle (Lu et al., 2021; Cubuk et al., 2021; Yao et al., 2020; Nikolakaki and Giannakouros, 2020). The SARS-CoV-2 N protein appears to localize at viral replication transcription complexes (RTCs) and facilitate viral RNA synthesis by forming phase-separated condensates with RNA-dependent RNA-polymerase complex components nsp7, nsp8, and nsp12 (Savastano et al., 2020; Verheije et al., 2010; Hillen et al., 2020). Additionally, the N protein from the measles virus has been reported to undergo LLPS to assemble genomic RNA into a rigid helical

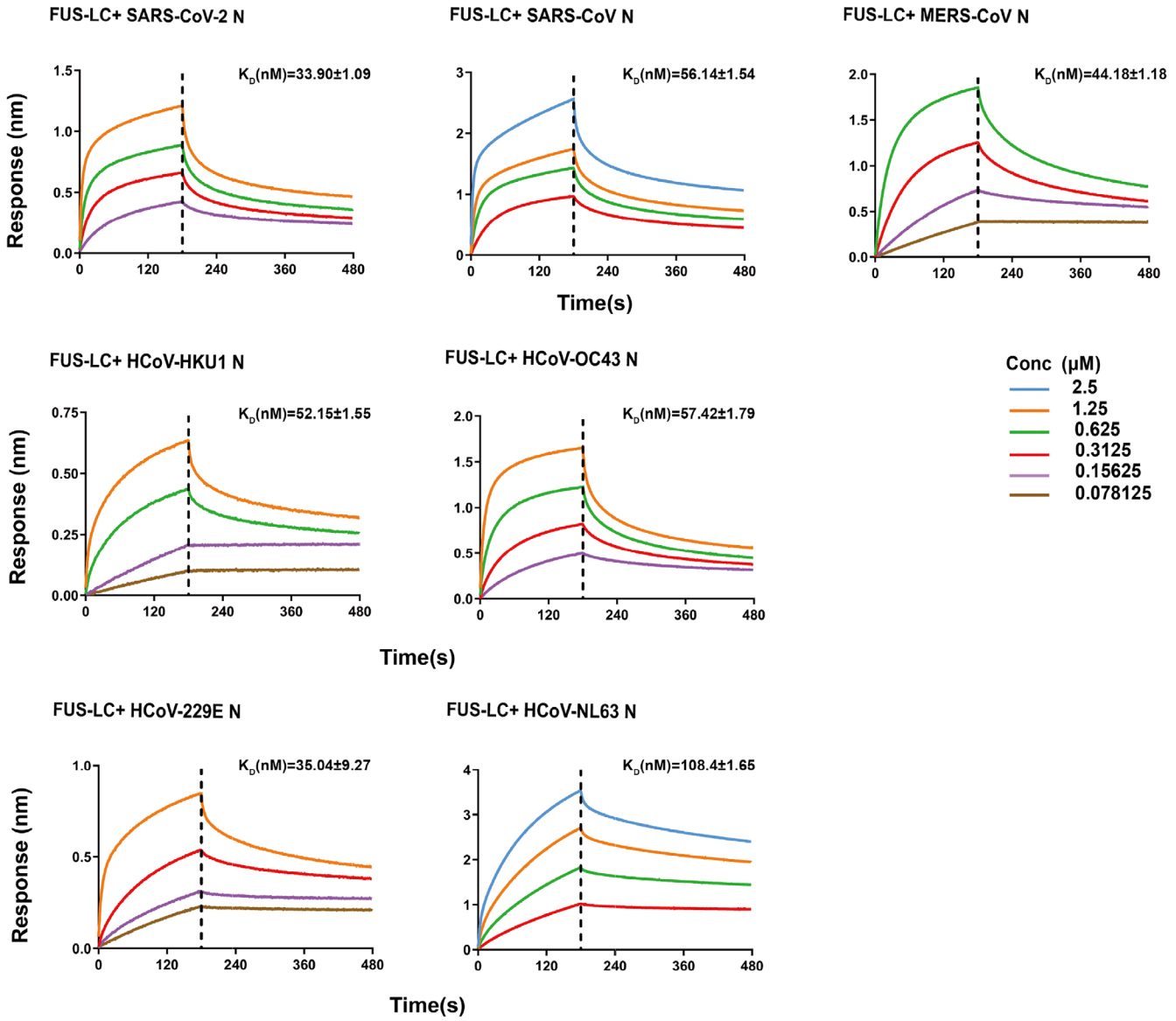

FIGURE 5 N protein directly binds to FUS-LC. Binding affinity of FUS-LC with seven homologous N proteins determined by BLI assay. The association and dissociation profiles of FUS-LC to N protein were divided by a vertical dash line. FUS-LC was fixed to the sensor, and different concentration of N protein used are indicated. The determined equilibrium constant (K_D) rates are labeled.

nucleocapsid (Milles et al., 2016; Guseva et al., 2020). These findings suggest that LLPS of the N protein plays a critical role in viral RNA replication, genome packaging, and virion assembly. In this study, we report that N proteins from various HCoVs can undergo LLPS, forming liquid-like droplets *in vitro*. This suggests that LLPS may serve as a general mechanism for N protein function in different HCoVs. However, various N proteins exhibit distinct LLPS profiles under different *in vitro* conditions, implying that individual HCoVs may have evolved to exploit these properties in a context-dependent manner. The ability of several different N proteins to phase separate in the presence of RNA further supports the notion that LLPS may be involved in viral genome packaging for different HCoVs. Nonetheless, more research is needed to clarify the molecular mechanisms through which N proteins from various HCoVs use LLPS to recruit RTC-related components to viral genomic RNA replication sites, recognize genomic RNA, and utilize the viral packaging signal to modulate N protein phase separation and promote the packaging of single genomes into virions.

Previous studies have shown that the SARS-CoV-2 N protein can partition into liquid-like condensates composed of SG proteins. It can further impair the dynamic properties of liquid droplets through inter-protein interaction and induce SG solidification (Luo et al., 2021; Li et al., 2022). Importantly, SG solidification is a key pathological event in NDs (Wolozin and Ivanov, 2019; Marcelo

et al., 2021; Khalfallah et al., 2018; Duan et al., 2019; Molliex et al., 2015; Zhang et al., 2018, 2020). Moreover, viral invasion into the nervous system has been linked to the pathogenesis and clinical onset of human NDs (Zhou et al., 2013; Bastian et al., 1972; Jang et al., 2009; Eimer et al., 2018; Readhead et al., 2018; Marreiros et al., 2020; Balin and Hudson, 2018). For instance, H1N1 influenza virus disrupts cellular proteostasis, causing α-synuclein (α-syn) aggregation and potentially triggering synucleinopathy (Marreiros et al., 2020). Extracellular herpesviridae viruses have been suggested to initiate amyloid β deposition and accelerate Alzheimer's disease (AD) progression (Eimer et al., 2018). Clinical correlations between SARS-CoV-2 infection and Parkinson's disease (PD) onset have also been reported (Cohen et al., 2020; Faber et al., 2020; Calculli et al., 2023; Antonini et al., 2020; Santos-Garcia et al., 2020). Another study has demonstrated that interactions between the SARS-CoV-2 N protein and α-syn can expedite α-syn amyloid formation, indicating a potential link between SARS-CoV-2 infections and PD (Semerdzhiev et al., 2022). Our *in vitro* data show that different N proteins of HCoVs can directly interact with the SG-containing protein FUS, accelerating the liquid-to-solid phase transition and amyloid aggregation of FUS. This suggests a potential risk of various HCoVs inducing pathological protein aggregation associated with NDs. Notably, the phase separation capability of different N proteins does not strongly correlate with their activities in promoting FUS aggregation. For example, NL63, which demonstrates relatively weak LLPS capability, exhibits a strong propensity to induce FUS aggregation. This implies that different N proteins may utilize distinct regions to mediate homotypic interactions between N proteins and heterotypic interactions between FUS and N proteins. Further in-depth investigation of these regions is warranted. Additionally, future studies should examine the functional consequences of these interactions in the context of viral infection and replication, as well as explore the potential therapeutic implications of targeting N protein interactions with host proteins.

4 | EXPERIMENTAL PROCEDURES

4.1 | Phylogenetic analysis

For sequence alignment, sequences of seven N proteins from human coronavirus were aligned using ClustalW (https://www.genome.jp/tools-bin/clustalw) with default parameters. Neighbor-Joining phylogenetic trees were generated by MEGA (v.11.0.13) with JTT substitution model and 500 bootstrap replicates.

4.2 | Plasmid construction, protein expression and purification

For *E. coli* expression, all full-length human Coronavirus N proteins were cloned to vector pET28a with an N-terminal His_6 tag. Full-length FUS (residues 1–526) was cloned into pET32a vector with a HRV 3C protease cleavable N-terminal MBP-His tag and an EGFP C-terminal tag. FUS-LC (residues 1–163) was cloned into pET22b vectors with an N-terminal His_6 tag.

For protein purification, N protein from SARS-CoV-2 was induced to express in *E. coli* BL21 (DE3) after adding 1 mM IPTG. After induction, cells grew overnight at 16°C, then the cells were harvested and lysed in lysis buffer containing 50 mM Tris–HCl (pH 7.5), 500 mM NaCl, 4 mM β-mercaptoethanol, 2 mM PMSF and 100 μg/mL RNase A (Roche, 10,109,142,001). The cellular lysate was centrifugated to remove the precipitates and subjected to Ni column (GE Healthcare). The protein was eluted with 50 mM Tris–HCl (pH 7.5), 500 mM NaCl, and 250 mM imidazole and then concentrated and subjected to size-exclusion chromatography column (Superdex 200 16/300, GE Healthcare) in 50 mM Tris–HCl (pH 7.5), 100 mM NaCl and 2 mM DTT.

N protein from SARS-CoV was induced to express in *E. coli* BL21 (DE3) cells at 25°C for 16 h after induction with 500 μM IPTG. N protein from HCoV-OC43 and HCoV-NL63 was induced to express in *E. coli* BL21 (DE3) cells at 16°C for 16 h after induction with 500 μM IPTG. And N protein from MERS-CoV, HCoV-HKU1 and HCoV-229E was induced to express in *E. coli* BL21 (DE3) cells at 30°C for 16 h after induction with 500 μM IPTG. The subsequent protein purification protocol was the same as that of SARS-CoV-2 N protein described above.

Full-length FUS was overexpressed in BL21 (DE3) *E. coli* cells at 16°C for 16 h after induction with 500 μM IPTG. Then, cells were harvested and lysed with lysis buffer (50 mM Tris–HCl, 500 mM NaCl, pH 8.0, 10 mM imidazole, 4 mM β-mercaptoethanol, 1 mM PMSF, and 0.1 mg/mL RNase A). Cell pellet was removed after centrifugation (16,000 rpm, 4°C, 1 h) and supernatant was loaded into a Ni column (GE Healthcare, USA). Protein was eluted in an elution buffer (50 mM Tris–HCl, 500 mM NaCl, pH 8.0, 100 mM imidazole and 4 mM β-mercaptoethanol). MBP-His tag was cleaved off using a GST-tagged 3C precision protease during dialysis against FUS dialysis buffer (50 mM Tris–HCl, 1 M KCl, 10% glycerol, 4 mM β-mercaptoethanol, pH 7.4) for 4 h. The mixture was loaded onto a Ni column and a Glutathione Sepharose column (GE Healthcare, USA) to remove the MBP-His and protease. The protein was further purified over the size-exclusion chromatography column

(Superdex 200 16/300; GE Healthcare) in 50 mM Tris–HCl (pH 7.5), 500 mM KCl, 2 mM DTT and 10% glycerol.

FUS-LC was expressed in *E. coli* BL21 (DE3) and then induced with 0.5 mM IPTG at 16°C for 48 h. Cells were collected and lysed by sonication in 50 mM Tris–HCl (pH 8.0), 6 M guanidine hydrochloride on the ice. Cell pellet was removed by centrifugation (14,000 rpm, 4°C, 40 min) and then cell supernatant was loaded onto a Ni column after filtration. Protein was eluted in 50 mM Tris–HCl (pH 8.0), 6 M guanidine hydrochloride and 50 mM imidazole. Further the eluted protein was purified via high performance liquid chromatography (HPLC) (Agilent) and freeze dried by FreeZone lyophilizer (Thermo Fisher). FUS-LC powder was dissolved into 50 mM Tris–HCl (pH 8.0), 8 M urea and then desalted into 5 mM CAPS (pH 11.0) for long-term storage.

4.3 | Protein fluorescent labeling

All N proteins were desalted and resuspended in a solution containing 50 mM sodium phosphate (pH 7.0) and 200 mM sodium chloride. The QSY7 fluorophore, operating on the NHS ester reaction mechanism, was utilized to target primary amines (—NH_2) on the N-terminus of each polypeptide chain as well as on the side-chain of lysine residues. The proteins were then incubated with a 10-fold molar excess (10:1) of QSY7 (Invitrogen, Q10193) at 25°C for 1 h. Subsequently, the labeled proteins were further purified using a Superdex 75 10/300 size-exclusion chromatography column (GE Healthcare) in the same buffer. The unlabeled protein was then mixed with the fluorescent labeled protein with the molar ratio of 50:1 (unlabeled:labeled) for the following LLPS assay and confocal imaging (Wu et al., 2021; Gu et al., 2020, 2021; Hallegger et al., 2021).

4.4 | *In vitro* HiPPS profiling assay

For the HiPPS profiling assay, stock solutions containing 96 different LLPS-inducing reagents (Li et al., 2022), were prepared and stored separately. Aliquots of these solutions were allocated into a 96-well plate. A stock solution was prepared for different N proteins (100 μM) from human coronavirus. The Mosquito Crystallization Robot (SPT Labtech) was employed to dispense an ultra-low volume of N proteins (750 nL/drop) on a 96-well hanging-drop film (FAstal BioTech, China, CAS: 296), followed by mixing with 1:1 profiling solution. Subsequently, the 96-well film was inverted and adhered to a custom-made transparent, flat acrylic board or the back flat surface of a 96-well plate (Thermo Scientific, CAS: 167008). An optical microscope was employed for preliminary observation by monitoring the wells. The automatic imaging system of Operetta CLS high-content analysis system (PerkinElmer) was subsequently utilized to automatically scan and counts the number of droplets particles in each well. And each well would be scored based on the density and size of the droplets, which follows the previously published protocol (Li et al., 2022). For the protein phase separation score (PPS), 96 conditions were classified into 7 subzones (n1: A1–F8; n2: A9–F10; n3: A11–C12; n4: D11–F12; n5: G1–H5; n6: G6–H10; and n7: G11–H12). The value of each well in the subzone were averaged to obtain the score for each respective subzone (n1, n2, ..., n7). The PPS score was calculated as the sum of the scores for each subzone. PPS of N proteins were calculated based on the equation (where n indicates the serial number of the subzone):

$$\mathrm{pps}_{\mathrm{score}} = \sum_{n=1}^{7} \mathrm{Subzone}\ \overline{n}$$

4.4.1 | *In vitro* LLPS assay

In vitro co-LLPS experiments were performed at room temperature. The LLPS of N protein was induced by the addition of indicated volume ratio of PEG3350 (v/v%) in LLPS buffer containing 50 mM Tris–HCl (pH 7.5), 150 mM NaCl and 2 mM DTT. For the co-LLPS, N protein was incubated with FUS-EGFP in the buffer containing 50 mM Tris–HCl (pH 7.5), 150 mM NaCl. All imaged were captured within 5 min after LLPS induction. Finally, 4 μL of each sample was pipetted onto a coverslip and imaged using a Leica microscope.

4.4.2 | DIC and fluorescent imaging for protein LLPS

For imaging protein liquid droplets, samples were placed onto a glass slide and sealed with a coverslip. DIC images of LLPS and co-LLPS samples were captured using a Leica TCS SP8 microscope equipped with a 100× oil immersion objective at room temperature. Fluorescent images of protein samples were obtained with the same microscope, employing Leica TCS SP8 confocal imaging and a 100× oil immersion objective at a resolution of 2048 × 2048 pixels.

4.4.3 | Turbidity measurement

LLPS of N proteins and FUS were induced in the buffer as described above. Turbidity measurements were conducted at 600 nm in a 384-well plate with 20 μL samples using a Varioskan Flash spectral scanning multimode reader (Thermo Fisher).

4.4.4 | FUS phase transition and maturation assay

The samples contained 10 μM full-length FUS-EGFP in the presence or absence of 10 μM N protein in 50 mM Tris–HCl (pH 7.5), 150 mM NaCl. Twenty microliters samples were placed on the glass bottom of 384-well plates (Corning) and the plate was shaken at 900 rpm. Leica TCS SP8 confocal microscopy was used to record images and FRAP data at indicated time points by using a 100× objective (oil immersion) with Z-stacks over 3 μm. The experimental conditions of seven human coronaviruses N protein were consistent as described above.

4.4.5 | FRAP

All FRAP experiments were performed on FRAP module of the Leica TCS SP8 confocal microscopy with 100× objective (oil immersion). For *in vitro* FRAP assay, the time-lapse images were captured at wavelengths of 488 or 568 nm, with an acquisition resolution of 1024 × 1024 pixels. The bleaching area of the droplet was confined to a specific region and then subjected to full laser power for 2.58 s. Post-bleach images were acquired at a rate of one frame every 3 s. The intensity at each time point was corrected by referencing the intensity of a nearby unbleached region.

4.4.6 | ThT fluorescence assay

All ThT experiments were performed in buffer containing 50 mM Tris–HCl (pH 7.5), 150 mM NaCl, 50 μM ThT and 0.05% NaN_3 was incubated in 384-well plates (Corning) at 25°C. Each ThT sample was prepared to a volume of 60 μL containing FUS-LC (25 μM) and indicated concentrations of each N protein. ThT fluorescence was monitored using a Varioskan Flash spectral scanning multimode reader (Thermo Fisher Scientific) with excitation at 440 nm and emission at 485 nm at 25°C. The sample plate was shaken at 700 rpm for 10 s before each measurement of ThT fluorescent intensity. Five replicates were performed for each sample.

4.4.7 | Negative-staining TEM

Five microliters of each sample was transferred to carbon-coated grids for 1 min and stained with 5 μL uranyl acetate (2%, v/v) for 45 s. Removing and drying the excess buffer on grids before acquiring TEM images. Grids were further assessed by using Tecnai G2 Spirit TEM operated at an accelerating voltage of 120 kV. Images were recorded using a 4 K × 4 K charge-coupled device camera (BM-Eagle, FEI Tecnai).

4.4.8 | BLI assay

The binding kinetics of the FUS-LC to N proteins of Human coronaviruses were measured by BLI on an ForteBio Octet RED96 system (Pall ForteBio LLC). Experiments were performed at room temperature using the assay buffer of 50 mM Tris–HCl, 150 mM NaCl, pH 7.5. FUS-LC was firstly biotinylated by incubating 0.5–1 mg/mL proteins with biotin at a molar ratio of protein:biotin of 2:3 at room temperature for 30 min, then the excess biotins were removed by desalting column (Zeba Spin Desalting Columns, Thermo). Then biotinylated FUS-LC was immobilized onto streptavidin biosensors (ForteBio) individually, and incubated with a series concentrations of N proteins as indicated in the figure. The resulting curves were corrected using the blank reference and analyzed by the ForteBio Data Analysis software 9.0.

4.4.9 | Quantification and statistical analysis

All experiments were performed in replicates, with statistical parameters such as definitions and exact values of n (number of biological repeats), distributions, and deviations detailed in the corresponding figures and figure legends. Statistical analyses were conducted using Microsoft Excel or GraphPad Prism software. All statistic values were displayed as mean ± SD. The statistical significance in this study is determined by the unpaired, two-tailed Student's *t*-test.

AUTHOR CONTRIBUTIONS

Hui Dong and Dan Li designed the project. Hui Dong, Shenqing Zhang, Zibo Liu, and Julie Jalin purified seven recombinant N proteins from human coronaviruses and FUS protein. Hui Dong and Hong Zhang performed the *in vitro* characterization of protein phase separation and aggregation. Runhan Wang and Ziqi He performed the BLI experiments. All the authors are involved in analyzing the data and contributed to manuscript discussion and editing. Hui Dong and Dan Li wrote the manuscript.

ACKNOWLEDGMENTS

We thank staff members of the National Facility for Protein Science in Shanghai, Zhangjiang Laboratory, China, for providing technical support and assistance in BLI data collection. This work was supported by the National Natural Science Foundation (NSF) of China (32170683 to Dan Li).

CONFLICT OF INTEREST STATEMENT

The authors declare no competing interests.

DATA AVAILABILITY STATEMENT

All data are contained within the manuscript and supporting materials.

ORCID

Hong Zhang https://orcid.org/0009-0002-2951-8631

REFERENCES

Antonini A, Leta V, Teo J, Chaudhuri KR. Outcome of Parkinson's disease patients affected by COVID-19. Mov Disord. 2020;35:905–8.

Balin BJ, Hudson AP. Herpes viruses and Alzheimer's disease: new evidence in the debate. Lancet Neurol. 2018;17:839–41.

Banani SF, Lee HO, Hyman AA, Rosen MK. Biomolecular condensates: organizers of cellular biochemistry. Nat Rev Mol Cell Biol. 2017;18:285–98.

Bastian FO, Rabson AS, Yee CL, Tralka TS. Herpesvirus hominis: isolation from human trigeminal ganglion. Science. 1972;178:306–7.

Calculli A, Bocci T, Porcino M, Avenali M, Casellato C, Arceri S, et al. Parkinson disease following COVID-19: report of six cases. Eur J Neurol. 2023;30:1272–80.

Cascarina SM, Ross ED. A proposed role for the SARS-CoV-2 nucleocapsid protein in the formation and regulation of biomolecular condensates. FASEB J. 2020;34:9832–42.

Chan JF, Kok K-H, Zhu Z, Chu H, To KK-W, Yuan S, et al. Genomic characterization of the 2019 novel human-pathogenic coronavirus isolated from a patient with atypical pneumonia after visiting Wuhan. Emerg Microbes Infect. 2020;9:221–36.

Chang CK, Hou MH, Chang CF, Hsiao CD, Huang TH. The SARS coronavirus nucleocapsid protein—forms and functions. Antiviral Res. 2014;103:39–50.

Chang CK, Hsu YL, Chang YH, Chao FA, Wu MC, Huang YS, et al. Multiple nucleic acid binding sites and intrinsic disorder of severe acute respiratory syndrome coronavirus nucleocapsid protein: implications for ribonucleocapsid protein packaging. J Virol. 2009;83:2255–64.

Chen CY, Chang CK, Chang YW, Sue SC, Bai HI, Riang L, et al. Structure of the SARS coronavirus nucleocapsid protein RNA-binding dimerization domain suggests a mechanism for helical packaging of viral RNA. J Mol Biol. 2007;368:1075–86.

Chen B, Tian EK, He B, Tian L, Han R, Wang S, et al. Overview of lethal human coronaviruses. Signal Transduct Target Ther. 2020;5:89.

Cohen ME, Eichel R, Steiner-Birmanns B, Janah A, Ioshpa M, Bar-Shalom R, et al. A case of probable Parkinson's disease after SARS-CoV-2 infection. Lancet Neurol. 2020;19:804–5.

Coronaviridae Study Group of the International Committee on Taxonomy of Viruses. The species severe acute respiratory syndrome-related coronavirus: classifying 2019-nCoV and naming it SARS-CoV-2. Nat Microbiol. 2020;5:536–44.

Cubuk J, Alston JJ, Incicco JJ, Singh S, Stuchell-Brereton MD, Ward MD, et al. The SARS-CoV-2 nucleocapsid protein is dynamic, disordered, and phase separates with RNA. Nat Commun. 2021;12:1936.

Decker CJ, Parker R. P-bodies and stress granules: possible roles in the control of translation and mRNA degradation. Cold Spring Harb Perspect Biol. 2012;4:a012286.

Dolliver SM, Kleer M, Bui-Marinos MP, Ying S, Corcoran JA, Khaperskyy DA. Nsp1 proteins of human coronaviruses HCoV-OC43 and SARS-CoV2 inhibit stress granule formation. PLoS Pathog. 2022;18:e1011041.

Drosten C, Günther S, Preiser W, van der Werf S, Brodt HR, Becker S, et al. Identification of a novel coronavirus in patients with severe acute respiratory syndrome. N Engl J Med. 2003;348:1967–76.

Duan Y, du A, Gu J, Duan G, Wang C, Gui X, et al. PARylation regulates stress granule dynamics, phase separation, and neurotoxicity of disease-related RNA-binding proteins. Cell Res. 2019;29:233–47.

Eimer WA, Vijaya Kumar DK, Navalpur Shanmugam NK, Rodriguez AS, Mitchell T, Washicosky KJ, et al. Alzheimer's disease-associated beta-amyloid is rapidly seeded by Herpesviridae to protect against brain infection. Neuron. 2018;99:56–63 e53.

Faber I, Brandão PRP, Menegatti F, de Carvalho Bispo DD, Maluf FB, Cardoso F. Coronavirus disease 2019 and parkinsonism: a non-post-encephalitic case. Mov Disord. 2020;35:1721–2.

Fung TS, Liu DX. Human coronavirus: host–pathogen interaction. Annu Rev Microbiol. 2019;73:529–57.

Gu J, Liu Z, Zhang S, Li Y, Xia W, Wang C, et al. Hsp40 proteins phase separate to chaperone the assembly and maintenance of membraneless organelles. Proc Natl Acad Sci U S A. 2020;117:31123–33.

Gu J, Wang C, Hu R, Li Y, Zhang S, Sun Y, et al. Hsp70 chaperones TDP-43 in dynamic, liquid-like phase and prevents it from amyloid aggregation. Cell Res. 2021;31:1024–7.

Guseva S, Milles S, Jensen MR, Salvi N, Kleman JP, Maurin D, et al. Measles virus nucleo- and phosphoproteins form liquid-like phase-separated compartments that promote nucleocapsid assembly. Sci Adv. 2020;6:eaaz7095.

Hallegger M, Chakrabarti AM, Lee FCY, Lee BL, Amalietti AG, Odeh HM, et al. TDP-43 condensation properties specify its RNA-binding and regulatory repertoire. Cell. 2021;184:4680–4696 e4622.

Hillen HS, Kokic G, Farnung L, Dienemann C, Tegunov D, Cramer P. Structure of replicating SARS-CoV-2 polymerase. Nature. 2020;584:154–6.

Iserman C, Roden CA, Boerneke MA, Sealfon RSG, McLaughlin GA, Jungreis I, et al. Genomic RNA elements drive phase separation of the SARS-CoV-2 nucleocapsid. Mol Cell. 2020;80:1078–1091 e1076.

Jang HM, Boltz D, Sturm-Ramirez K, Shepherd KR, Jiao Y, Webster R, et al. Highly pathogenic H5N1 influenza virus can enter the central nervous system and induce neuroinflammation and neurodegeneration. P Natl Acad Sci USA. 2009;106:14063–8.

Jung J-H, Barbosa AD, Hutin S, Kumita JR, Gao M, Derwort D, et al. A prion-like domain in ELF3 functions as a thermosensor in Arabidopsis. Nature. 2020;585:256–60.

Kato M, Han TW, Xie S, Shi K, du X, Wu LC, et al. Cell-free formation of RNA granules: low complexity sequence domains form dynamic fibers within hydrogels. Cell. 2012;149:753–67.

Khalfallah Y, Kuta R, Grasmuck C, Prat A, Durham HD, Vande Velde C. TDP-43 regulation of stress granule dynamics in neurodegenerative disease-relevant cell types. Sci Rep. 2018;8:7551.

Li Y, Gu J, Liu C, Li D. A high-throughput method for exploring the parameter space of protein liquid-liquid phase separation. Cell Rep Phys Sci. 2022;3:100764.

Li Y, Gu J, Wang C, Hu J, Zhang S, Liu C, et al. Hsp70 exhibits a liquid-liquid phase separation ability and chaperones condensed FUS against amyloid aggregation. iScience. 2022;25:104356.

Li Y, Lu S, Gu J, Xia W, Zhang S, Zhang S, et al. SARS-CoV-2 impairs the disassembly of stress granules and promotes ALS-associated amyloid aggregation. Protein Cell. 2022;13:602–14.

Lu S, Ye Q, Singh D, Cao Y, Diedrich JK, Yates JR III, et al. The SARS-CoV-2 nucleocapsid phosphoprotein forms mutually exclusive condensates with RNA and the membrane-associated M protein. Nat Commun. 2021;12:502.

Luo L, Li Z, Zhao T, Ju X, Ma P, Jin B, et al. SARS-CoV-2 nucleocapsid protein phase separates with G3BPs to disassemble stress granules and facilitate viral production. Sci Bull. 2021;66:1194–204.

Marcelo A, Koppenol R, de Almeida LP, Matos CA, Nóbrega C. Stress granules, RNA-binding proteins and polyglutamine diseases: too much aggregation? Cell Death Dis. 2021;12:592.

Marreiros R, Müller-Schiffmann A, Trossbach SV, Prikulis I, Hänsch S, Weidtkamp-Peters S, et al. Disruption of cellular proteostasis by H1N1 influenza A virus causes alpha-synuclein aggregation. Proc Natl Acad Sci U S A. 2020;117:6741–51.

Mathieu C, Pappu RV, Taylor JP. Beyond aggregation: pathological phase transitions in neurodegenerative disease. Science. 2020;370:56–60.

Milles S, Jensen MR, Communie G, Maurin D, Schoehn G, Ruigrok RWH, et al. Self-assembly of measles virus nucleocapsid-like particles: kinetics and RNA sequence dependence. Angew Chem Int Ed Engl. 2016;55:9356–60.

Molliex A, Temirov J, Lee J, Coughlin M, Kanagaraj AP, Kim HJ, et al. Phase separation by low complexity domains promotes stress granule assembly and drives pathological fibrillization. Cell. 2015;163:123–33.

Murray DT, Kato M, Lin Y, Thurber KR, Hung I, McKnight SL, et al. Structure of FUS protein fibrils and its relevance to self-assembly and phase separation of low-complexity domains. Cell. 2017;171:615–627 e616.

Naumann M, Pal A, Goswami A, Lojewski X, Japtok J, Vehlow A, et al. Impaired DNA damage response signaling by FUS-NLS mutations leads to neurodegeneration and FUS aggregate formation. Nat Commun. 2018;9:335.

Nikolakaki E, Giannakouros T. SR/RS motifs as critical determinants of coronavirus life cycle. Front Mol Biosci. 2020;7:219.

Obradovic Z, Peng K, Vucetic S, Radivojac P, Brown CJ, Dunker AK. Predicting intrinsic disorder from amino acid sequence. Proteins. 2003;53(Suppl 6):566–72.

Patel A, Lee HO, Jawerth L, Maharana S, Jahnel M, Hein MY, et al. A liquid-to-solid phase transition of the ALS protein FUS accelerated by disease mutation. Cell. 2015;162:1066–77.

Perdikari TM, Murthy AC, Ryan VH, Watters S, Naik MT, Fawzi NL. SARS-CoV-2 nucleocapsid protein phase-separates with RNA and with human hnRNPs. EMBO J. 2020;39:e106478.

Quiroz FG, Fiore VF, Levorse J, Polak L, Wong E, Pasolli HA, et al. Liquid–liquid phase separation drives skin barrier formation. Science. 2020;367:eaax9554.

Readhead B, Haure-Mirande JV, Funk CC, Richards MA, Shannon P, Haroutunian V, et al. Multiscale analysis of independent Alzheimer's cohorts finds disruption of molecular, genetic, and clinical networks by human herpesvirus. Neuron. 2018;99:64–82 e67.

Rhoads SN, Monahan ZT, Yee DS, Shewmaker FP. The role of post-translational modifications on prion-like aggregation and liquid-phase separation of FUS. Int J Mol Sci. 2018;19:886.

Santos-Garcia D, Oreiro M, Pérez P, Fanjul G, González JMP, Painceiras MJF, et al. Impact of coronavirus disease 2019 pandemic on Parkinson's disease: a cross-sectional survey of 568 Spanish patients. Mov Disord. 2020;35:1712–6.

Savastano A, de Opakua AI, Rankovic M, Zweckstetter M. Nucleocapsid protein of SARS-CoV-2 phase separates into RNA-rich polymerase-containing condensates. Nat Commun. 2020;11:6041.

Semerdzhiev SA, Fakhree MAA, Segers-Nolten I, Blum C, Claessens M. Interactions between SARS-CoV-2 N-protein and alpha-synuclein accelerate amyloid formation. ACS Chem Neurosci. 2022;13:143–50.

Snijder EJ, van der Meer Y, Zevenhoven-Dobbe J, Onderwater JJM, van der Meulen J, Koerten HK, et al. Ultrastructure and origin of membrane vesicles associated with the severe acute respiratory syndrome coronavirus replication complex. J Virol. 2006;80:5927–40.

Su X, Ditlev JA, Hui E, Xing W, Banjade S, Okrut J, et al. Phase separation of signaling molecules promotes T cell receptor signal transduction. Science. 2016;352:595–9.

Sun Y, Zhang S, Hu J, Tao Y, Xia W, Gu J, et al. Molecular structure of an amyloid fibril formed by FUS low-complexity domain. iScience. 2022;25:103701.

Verheije MH, Hagemeijer MC, Ulasli M, Reggiori F, Rottier PJM, Masters PS, et al. The coronavirus nucleocapsid protein is dynamically associated with the replication-transcription complexes. J Virol. 2010;84:11575–9.

V'Kovski P, Kratzel A, Steiner S, Stalder H, Thiel V. Coronavirus biology and replication: implications for SARS-CoV-2. Nat Rev Microbiol. 2021;19:155–70.

Wolozin B, Ivanov P. Stress granules and neurodegeneration. Nat Rev Neurosci. 2019;20:649–66.

Wu X, Ganzella M, Zhou J, Zhu S, Jahn R, Zhang M. Vesicle tethering on the surface of phase-separated active zone condensates. Mol Cell. 2021;81:13–24 e17.

Wu A, Peng Y, Huang B, Ding X, Wang X, Niu P, et al. Genome composition and divergence of the novel coronavirus (2019-nCoV) originating in China. Cell Host Microbe. 2020;27:325–8.

Yang H, Rao Z. Structural biology of SARS-CoV-2 and implications for therapeutic development. Nat Rev Microbiol. 2021;19:685–700.

Yao H, Song Y, Chen Y, Wu N, Xu J, Sun C, et al. Molecular architecture of the SARS-CoV-2 virus. Cell. 2020;183:730–738 e713.

Zaki AM, van Boheemen S, Bestebroer TM, Osterhaus AD, Fouchier RA. Isolation of a novel coronavirus from a man with pneumonia in Saudi Arabia. N Engl J Med. 2012;367:1814–20.

Zeng M, Chen X, Guan D, Xu J, Wu H, Tong P, et al. Reconstituted postsynaptic density as a molecular platform for understanding synapse formation and plasticity. Cell. 2018;174:1172–1187. e1116.

Zeng W, Liu G, Ma H, Zhao D, Yang Y, Liu M, et al. Biochemical characterization of SARS-CoV-2 nucleocapsid protein. Biochem Biophys Res Commun. 2020;527:618–23.

Zhang Y-J, Gendron TF, Ebbert MTW, O'Raw AD, Yue M, Jansen-West K, et al. Poly(GR) impairs protein translation and stress granule dynamics in C9orf72-associated frontotemporal dementia and amyotrophic lateral sclerosis. Nat Med. 2018;24:1136–42.

Zhang H, Ji X, Li P, Liu C, Lou J, Wang Z, et al. Liquid-liquid phase separation in biology: mechanisms, physiological functions and human diseases. Sci China Life Sci. 2020;63:953–85.

Zhang JZ, Lu TW, Stolerman LM, Tenner B, Yang JR, Zhang JF, et al. Phase separation of a PKA regulatory subunit controls cAMP compartmentation and oncogenic signaling. Cell. 2020;182:1531–1544.e1515.

Zhang G, Wang Z, Du Z, Zhang H. mTOR regulates phase separation of PGL granules to modulate their Autophagic degradation. Cell. 2018;174:1492–1506.e1422.

Zhang X, Wang F, Hu Y, Chen R, Meng D, Guo L, et al. In vivo stress granule misprocessing evidenced in a FUS knock-in ALS mouse model. Brain. 2020;143:1350–67.

Zheng Z, Wang S, Xu Z, Fu Y, Wang Y. SARS-CoV-2 nucleocapsid protein impairs stress granule formation to promote viral replication. Cell Discovery. 2021;7:38.

Zhou L, Miranda-Saksena M, Saksena NK. Viruses and neurodegeneration. Virol J. 2013;10:172.

Zhou P, Yang XL, Wang XG, Hu B, Zhang L, Zhang W, et al. A pneumonia outbreak associated with a new coronavirus of probable bat origin. Nature. 2020;579:270–3.

Zhu SB, Gu J, Yao J, Li Y, Zhang Z, Xia W, et al. Liquid–liquid phase separation of RBGD2/4 is required for heat stress resistance in Arabidopsis. Dev Cell. 2022;57:583–597.e6.

SUPPORTING INFORMATION

Additional supporting information can be found online in the Supporting Information section at the end of this article.

How to cite this article: Dong H, Zhang H, Jalin J, He Z, Wang R, Huang L, et al. Nucleocapsid proteins from human coronaviruses possess phase separation capabilities and promote FUS pathological aggregation. Protein Science. 2023;32(12):e4826. https://doi.org/10.1002/pro.4826